Effects of density dependence of the effective pairing interaction on the first 2^+ excitations and quadrupole moments of odd nuclei

S. V. Tolokonnikov
Kurchatov Institute, 123182 Moscow and Moscow Institute of Physics and Technology, 123098 Moscow, Russia

S. Kamerdzhiev and D. Voitenkov
Institute for Physics and Power Engineering, 249033 Obninsk, Russia

S. Krewald
Institut für Kernphysik, Forschungszentrum Jülich, DE-52425 Jülich, Germany

E. E. Saperstein
Kurchatov Institute, 123182 Moscow

(Received 12 August 2011; revised manuscript received 18 October 2011; published 27 December 2011)

Excitation energies and transition probabilities of the first 2^+ excitations in even tin and lead isotopes as well as the quadrupole moments of odd neighbors of these isotopes are calculated within the self-consistent theory of finite Fermi systems based on the energy density functional by Fayans *et al.* [Nucl. Phys. A **676**, 49 (2000)]. The effect of the density dependence of the effective pairing interaction is analyzed in detail by comparing results obtained with volume and surface pairing. The effect is found to be noticeable. For example, the 2^+ energies are systematically higher at 200–400 keV for the volume paring as compared with the surface-pairing case. However, on the average, both models reasonably agree with the data. Quadrupole moments of odd-neutron nuclei are very sensitive to the single-particle energy of the state λ under consideration owing to the Bogolyubov factor $(u_\lambda^2 - v_\lambda^2)$. A reasonable agreement with experiment for the quadrupole moments has been obtained for the most part of odd nuclei considered. The method used gives a reliable possibility to predict quadrupole moments of unstable odd nuclei, including very neutron rich ones.

DOI: 10.1103/PhysRevC.84.064324 PACS number(s): 21.10.Jx, 21.10.Ky, 21.10.Re, 21.30.Fe

I. INTRODUCTION

Presently, there are two theoretical approaches which can quantitatively describe the bulk properties of nuclear isotope chains with a small number of effective coupling constants: self-consistent mean-field theories and density-functional theory. The successes and open problems of the mean-field approaches are reviewed in Refs. [1–3]. The Kohn-Sham density functional theory was originally proposed for chemistry and solids [4,5]. Important theoretical developments have been made: An extension of the Hohenberg-Kohn theorem to pairing degrees of freedom by Oliveira, Gross, and Kohn allowed studies of superfluids [6] and the generalization of functional theory to study excited states made it possible to investigate the electromagnetic response of correlated electron materials [7]. In nuclear physics, a self-consistent theory of finite Fermi systems (TFFS) was derived by Khodel and Saperstein [8] on the basis of the TFFS by Migdal [9] supplemented with the many-body theory self-consistency relation [10] for the nucleon mass operator. As was shown in Ref. [11], the self-consistent TFFS for nuclei without pairing can be reformulated as a particular version of the density functional method with a rather complicated ρ dependence of the energy functional. It contains also τ-dependent terms but with rather small strength resulting for the effective mass in a small difference of $|m^*_{n,p}(r) - m| \simeq 0.05m$. In a series of articles by Fayans *et al.* [12,13] (see also [14] and references therein), the energy density functional (EDF) method was generalized for superfluid nuclei. Just as in the original Kohn-Sham approach, the identity $m^* = m$ was imposed. A fractional form of the density dependence for the central part of the normal component of the EDF was introduced. The coordinate dependence of it resembled that of Ref. [11] but the functional form was much simpler, making the self-consistent QRPA calculations easier. Note that a recent generalization of the Skyrme force in Ref. [15] contains a new term with a density dependence resembling that in Ref. [14]. In addition, the velocity-dependent force in Ref. [15] is rather weak, leading to the effective mass $m^* \simeq 0.9m$. Thus, the self-consistent mean-field approaches may eventually converge with the density functional methods.

The nonrelativistic versions of the self-consistent mean-field theories introduce three-nucleon forces which are often expressed as a density-dependent two-body interaction. In general, one assumes a fractional power of the density dependence. Recent advances in effective field theory open the possibility to connect the density functional with the effective two- and three-nucleon systems which are determined from two-nucleon scattering and few-nucleon reactions. Reviews about the current status of such attempts are given in Refs. [16,17].

The question arises of whether the pairing interaction should have an analogous dependence on the normal nuclear density. Several studies derived pairing interactions from free two-nucleon interactions. Baldo *et al.* solved the gap equation in semi-infinite nuclear matter [18], nuclear slab [19], and finite

nuclei [20,21]. The Paris and Argonne v_{18} NN potentials were used, the results being almost identical. To make results more appropriate for practical nuclear self-consistent calculations dealing with pairing in a model space, the pairing problem was treated in a two-step way. The gap equation was solved in a model space with limiting energy $E_0 = 30$–40 MeV with the use of the effective pairing interaction. The latter is found in the subsidiary subspace in terms of a free NN potential. For all systems under consideration and the two NN potentials the effective pairing interaction found is much stronger, up to ten times, at the surface than inside. The Milan group concentrated on the ^{120}Sn nucleus, a traditional benchmark for the nuclear pairing problem, and solved the gap equation starting from the Argonne v_{14} potential [22]. In addition to the free NN interaction, they included corrections owing to exchange with low-lying surface vibrations ("phonons") [23] and high-lying excitations, mainly spin-dependent ones [24]. In the last article, a local three-parameter density-dependent effective pairing interaction is constructed for the model space with $E_0 = 60$ MeV, which reproduces approximately exact gap values. Qualitatively, it is similar to that described above. Without all corrections, it consists of a strong surface attraction and very weak attraction inside. Taking into account of the phonon exchange makes the inner interaction repulsive. At last, inclusion of the spin-dependent excitations makes the inner repulsion rather strong. Thus, the *ab initio* calculations of the effective pairing interaction predict essential density dependence with strong surface attraction.

As an alternative to consideration of the gap equation with complete realistic NN interactions, Bulgac and Yu used the fact that this equation depends mainly on the low-k behavior of NN force which can be approximated with a rather simple analytical function. It helped to develop a renormalization scheme for the gap equation without any cutoff in terms of zero-range interactions with explicit coordinate dependence of the effective pairing interaction and to suggest an EDF for superfluid nuclei [25,26].

The calculations by Fayans *et al.* employed both volume-pairing and surface-pairing interactions. The binding energies and the proton and neutron separation energies were found to be insensitive to the type of pairing force used. However, the odd-even staggering of charge radii can be quantitatively reproduced only if the strong density dependence of the pairing force is introduced [14].

In this work, we investigate the excitation energies and transition rates of the low-lying 2^+ states in spherical nuclei with the aim to analyze the sensitivity of those observables to the details of the pairing interaction. We compare two opposite limits, the "volume pairing" with density-independent effective pairing interaction $\mathcal{F}^\xi$ and the case of the function $\mathcal{F}^\xi$ with the surface dominance. The latter is named for brevity the "surface pairing." Several sets of calculations of these characteristics of the first 2^+ excitations were carried out recently within the QRPA method with Skyrme force [27,28] and within the generator coordinate method with the Gogny force [29]. No systematic analysis of the density dependence of the pairing force was performed in these studies. Dealing with low-laying quadrupole excitations, it is natural to include into analysis also quadrupole moments of odd nuclei which give test of static quadrupole polarization.

In this paper, we use the EDF method [14] with the functional DF3-a [30]. In the latter the spin-orbit and effective tensor terms of the original functional DF3 [13,14] were modified. All the QRPA-like TFFS equations are solved in the self-consistent basis $(\varepsilon_\lambda, \varphi_\lambda)$ obtained within the EDF method with the functional DF3-a.

II. BRIEF OUTLINE OF THE FORMALISM

For completeness, we describe shortly the EDF method of Ref. [14] using mainly the notation of Ref. [31]. In this method, the ground-state energy of a nucleus is considered a functional of normal and anomalous densities,

$$E_0 = \int \mathcal{E}[\rho_n(\mathbf{r}), \rho_p(\mathbf{r}), \nu_n(\mathbf{r}), \nu_p(\mathbf{r})]d^3r. \tag{1}$$

The normal part of the EDF $\mathcal{E}_{\rm norm}$ contains the central, spin-orbit, and effective tensor nuclear terms and Coulomb interaction term for protons. The main, central-force, term of $\mathcal{E}_{\rm norm}$ is finite in range with Yukawa-type coordinate dependence. It is convenient to extract the $\delta(\mathbf{r}-\mathbf{r}')$-term from the Yukawa function separating the rest of

$$D(\mathbf{r}-\mathbf{r}') = \frac{1}{4\pi r_{\rm c}^2|\mathbf{r}-\mathbf{r}'|}\exp\left(-\frac{|\mathbf{r}-\mathbf{r}'|}{r_{\rm c}}\right) - \delta(\mathbf{r}-\mathbf{r}') \tag{2}$$

to generate the "surface" part $\mathcal{E}^{\rm s}$, which vanishes in infinite matter with $\rho(\mathbf{r}) = {\rm const}$. The Yukawa radius $r_{\rm c}$ is taken the same for the isoscalar and isovector channels. The "volume" part of the EDF, $\mathcal{E}^{\rm v}(\rho)$, is taken in Refs. [13,14,31] as a fractional function of densities $\rho_+ = \rho_n + \rho_p$ and $\rho_- = \rho_n - \rho_p$:

$$\mathcal{E}^{\rm v}(\rho) = C_0\left[a_+^{\rm v}\frac{\rho_+^2}{2}f_+^{\rm v}(x) + a_-^{\rm v}\frac{\rho_-^2}{2}f_-^{\rm v}(x)\right], \tag{3}$$

where

$$f_\pm^{\rm v}(x) = \frac{1-h_{1\pm}^{\rm v}x}{1+h_{2\pm}^{\rm v}x}. \tag{4}$$

Here $x = \rho_+/(2\rho_0)$ is the dimensionless nuclear density where ρ_0 is the density of nucleons of one kind in equilibrium symmetric nuclear matter. The factor $C_0 = (dn/d\varepsilon_{\rm F})^{-1}$ in Eq. (3) is the usual TFFS normalization factor, inverse density of states at the Fermi surface.

To write down the surface term in a compact form similar to Eq. (3), the "tilde" operator was introduced in Ref. [31] denoting the following folding procedure:

$$\widetilde{\phi(\mathbf{r})} = \int D(\mathbf{r}-\mathbf{r}')\phi(\mathbf{r}')d\mathbf{r}'. \tag{5}$$

Then we obtain

$$\mathcal{E}^{\rm s}(\rho) = C_0\tfrac{1}{2}[a_+^{\rm s}(\rho_+ f_+^{\rm s})\widetilde{(f_+^{\rm s}\rho_+)} + a_-^{\rm s}(\rho_- f_-^{\rm s})\widetilde{(f_-^{\rm s}\rho_-)}], \tag{6}$$

where

$$f_\pm^{\rm s}(x) = \frac{1}{1+h_\pm^{\rm s}x}. \tag{7}$$

All the above parameters, $a^{\rm v}_{\pm}$, $a^{\rm s}_{\pm}$, $h^{\rm v}_{1\pm}h^{\rm v}_{2\pm}$, $h^{\rm s}_{\pm}$, are dimensionless.

In momentum space, the operator (2) reads

$$D(q) = -\frac{(qr_{\rm c})^2}{1+(qr_{\rm c})^2}. \tag{8}$$

In the small $r_{\rm c}$ limit it reduces to $D(q) = -(qr_{\rm c})^2$, and Eq. (6) could be simplified to a Skyrme-like form proportional to $(\nabla\rho)^2$.

The spin-orbit interaction reads

$$\mathcal{F}_{sl} = C_0 r_0^2(\kappa + \kappa'\boldsymbol{\tau}_1\boldsymbol{\tau}_2)[\nabla_1\delta(\mathbf{r}_1-\mathbf{r}_2)\times(\mathbf{p}_1-\mathbf{p}_2)] \cdot(\boldsymbol{\sigma}_1+\boldsymbol{\sigma}_2), \tag{9}$$

where the factor r_0^2 is introduced to make the spin-orbit parameters κ, κ' dimensionless. It can be expressed in terms of the above equilibrium density, $r_0^2 = [3/(8\pi\rho_0)]^{2/3}$.

In nuclei with partially occupied spin-orbit doublets, the so-called spin-orbit density exists,

$$\rho^{\tau}_{sl}(\mathbf{r}) = \sum_{\lambda} \mathbf{n}^{\tau}_{\lambda}\left\langle\phi^{\tau *}_{\lambda}(\mathbf{r})(\boldsymbol{\sigma}\mathbf{l})\phi^{\tau}_{\lambda}(\mathbf{r})\right\rangle, \tag{10}$$

where $\tau = n, p$ is the isotopic index and averaging over spin variables is carried out. As it is well known (see, e.g., Ref. [8]), a new term appears in the spin-orbit mean field induced by the tensor forces and the first harmonic $\hat{g}_1$ of the spin Landau-Migdal (LM) amplitude. We combine those contributions into an effective tensor force or first spin harmonic,

$$\mathcal{F}^s_1 = C_0 r_0^2(g_1 + g'_1\boldsymbol{\tau}_1\boldsymbol{\tau}_2)\delta(\mathbf{r}_1-\mathbf{r}_2)(\boldsymbol{\sigma}_1\boldsymbol{\sigma}_2)(\mathbf{p}_1\mathbf{p}_2). \tag{11}$$

In Table I, we present all parameters of the normal part of the EDF DF3-a we use. Note that the major part of these parameters is identical to the ones used in the DF3 functional [14]. With one exception, all parameters for the central force part remained the same and only the spin-orbit and the first spin harmonic are changed according to Ref. [30]. Application of the volume part (3) to equilibrium nuclear matter, with the equilibrium relation, that is, vanishing pressure $p(\rho) = \rho^2\partial(\mathcal{E}/\rho)/\partial\rho$, makes it possible to find the parameters $a^{\rm v}_+$, $h^{\rm v}_{1+}$, and $h^{\rm v}_{2+}$ in terms of the nuclear-matter density ρ_0, the chemical potential μ_0, and the compression modulus $K_0 = 9dp/d\rho$. The asymmetry energy parameter β_0 yields a relation between the constants $a^{\rm v}_-$, $h^{\rm v}_{1-}$, and $h^{\rm v}_{2-}$. They are given in the upper half of Table I. The radius r_0 introduced above is shown instead of ρ_0. The value used in Ref. [14] was recalibrated in Ref. [30] to obtain a more accurate description of nuclear charge radii [32]. One more remark should be made concerning the table. The "natural" TFFS normalizing factor $C_0 = 2\varepsilon_{0\rm F}/(3\rho_0) = 308.2$ MeV fm^3 corresponding to parameters of nuclear matter in the third column of the table differs from the one, $C_0 = 300$ MeV fm^3, recommended in the second edition of the Migdal's textbook on the TFFS [33]. To make a comparison with other articles within the TFFS, we recalculated all the strength parameters to the latter. It explains a small difference of some values in the second column in the table from the original those in Ref. [14]. An essential difference between DF3 and DF3-a functionals takes place for the "spin-dependent" sector in the bottom of the table. As we found in Ref. [30], the second one describes the spin-orbit splitting of doublets better.

TABLE I. Parameters of the normal part of the EDF.

Parameter	DF3 [14]	DF3-a [30]
μ_0 (MeV)	−16.05	−16.05
r_0 (fm)	1.147	1.145
K_0 (MeV)	200	200
β (MeV)	28.7	28.7
$a^{\rm v}_+$	−6.598	−6.575
$h^{\rm v}_{1+}$	0.163	0.163
$h^{\rm v}_{2+}$	0.724	0.725
$a^{\rm v}_-$	5.565	5.523
$h^{\rm v}_{1-}$	0	0
$h^{\rm v}_{2-}$	3.0	3.0
$a^{\rm s}_+$	−11.4	−11.1
$h^{\rm s}_+$	0.31	0.31
$a^{\rm s}_-$	−4.11	−4.10
$h^{\rm s}_-$	0	0
$r_{\rm c}$ (fm)	0.35	0.35
κ	0.216	0.190
κ'	0.077	0.077
g_1	0	0
g'_1	−0.123	−0.308

The anomalous component of the EDF [14] reads

$$\mathcal{E}_{\rm an}(\mathbf{r}) = \sum_{\tau}\mathcal{F}^{\xi,\tau\tau}(\mathbf{r};[\rho])|\nu^{\tau}(\mathbf{r})|^2, \tag{12}$$

where the effective pairing interaction reads

$$\mathcal{F}^{\xi} = C_0 f^{\xi} = C_0\left[f^{\xi}_{\rm ex} + h^{\xi}x^{2/3} + f^{\xi}_{\nabla}r_0^2(\nabla x)^2\right]. \tag{13}$$

The first two terms are similar to those in the TFFS [34,35] or in the SHFB method [36]. The third in Eq. (13) is a new one introduced in Ref. [13]. In this paper we use an approximate version of Eq. (13) with $f^{\xi}_{\nabla} = 0$. We compare two models for nuclear pairing: the "volume" pairing ($h^{\xi} = 0$) and the "surface" pairing where both the pairing parameters $f^{\xi}_{\rm ex}$ and h^{ξ} are nonzero. One more remark should be made concerning the pairing problem. In the approach of Ref. [14] pairing was considered in the coordinate representation explicitly, solving the Gorkov equations with the method developed in Ref. [37]. However, it was found that the results are practically equivalent to those obtained within a more simple BCS-like scheme using the gap $\Delta_{\lambda\lambda'} = \Delta_{\lambda}\delta_{\lambda\lambda'}$ in a sufficiently large model space, $\varepsilon_{\lambda} < E_{\rm max}$. We do not apply this method for nuclei close to the drip line for which the diagonal approximation does not work [14]. The effective pairing interaction (13) for the BCS approximation is a little stronger than that in the coordinate representation. In Sec. III, we investigate the theoretical errors in the observables owing to the choice of the cutoff energy $E_{\rm max}$.

Within the TFFS, the response of a nucleus to the external quadrupole field $V_0\exp(i\omega t)$ can be found in terms of the effective field. In systems with pairing correlations, the equation for the effective field can be written in a compact form as

$$\hat{V}(\omega) = \hat{V}_0(\omega) + \hat{\mathcal{F}}\hat{A}(\omega)\hat{V}(\omega), \tag{14}$$

where all the terms are matrices. In the standard TFFS notation [9], we have

$$\hat{V} = \begin{pmatrix} V \\ d_1 \\ d_2 \end{pmatrix}, \quad \hat{V}_0 = \begin{pmatrix} V_0 \\ 0 \\ 0 \end{pmatrix}, \tag{15}$$

$$\hat{\mathcal{F}} = \begin{pmatrix} \mathcal{F} & \mathcal{F}^{\omega\xi} & \mathcal{F}^{\omega\xi} \\ \mathcal{F}^{\xi\omega} & \mathcal{F}^{\xi} & \mathcal{F}^{\xi\omega} \\ \mathcal{F}^{\xi\omega} & \mathcal{F}^{\xi\omega} & \mathcal{F}^{\xi} \end{pmatrix}, \tag{16}$$

$$\hat{A}(\omega) = \begin{pmatrix} \mathcal{L}(\omega) & \mathcal{M}_1(\omega) & \mathcal{M}_2(\omega) \\ \mathcal{O}(\omega) & -\mathcal{N}_1(\omega) & \mathcal{N}_2(\omega) \\ \mathcal{O}(-\omega) & -\mathcal{N}_1(-\omega) & \mathcal{N}_2(-\omega) \end{pmatrix}, \tag{17}$$

where $\mathcal{L}, \mathcal{M}_1$, and so on stand for integrals over ε of the products of different combinations of the Green's function $G(\varepsilon)$ and two Gor'kov functios $F^{(1)}(\varepsilon)$ and $F^{(2)}(\varepsilon)$. They can be found in Ref. [9] and we write here only the first of them, which is of main importance for us,

$$\mathcal{L} = \int \frac{d\varepsilon}{2\pi i}[G(\varepsilon)G(\varepsilon+\omega) - F^{(1)}(\varepsilon)F^{(2)}(\varepsilon+\omega)]. \tag{18}$$

Isotopic indices in Eqs. (15)–(17) are omitted for brevity. In Eq. (16), $\mathcal{F}$ is the usual LM amplitude,

$$\mathcal{F} = \frac{\delta^2\mathcal{E}}{\delta\rho^2}, \tag{19}$$

whereas the amplitudes $\mathcal{F}^{\omega\xi} = \mathcal{F}^{\xi\omega}$ stand for the mixed second derivatives,

$$\mathcal{F}^{\omega\xi} = \frac{\delta^2\mathcal{E}}{\delta\rho\delta\nu}. \tag{20}$$

In the case of volume pairing, we have $\mathcal{F}^{\omega\xi} = 0$. The explicit form of the above equations and (18) is written for the case of the electric (t-even) symmetry we deal with. A static moment of an odd nucleus can be found in terms of the diagonal matrix element $\langle\lambda_0|V(\omega=0)|\lambda_0\rangle$ of the effective field over the state λ_0 of the odd nucleon.

The effective field operator $\hat{V}(\omega)$ has a pole in the excitation energy ω_s of the state $|s\rangle$ under consideration,

$$\hat{V}(\omega) = \frac{(\hat{V}_0\hat{A}(\omega_s)\hat{g}_{0s})\hat{g}_{0s}}{\omega-\omega_s} + \hat{V}_R(\omega). \tag{21}$$

The quantity $\hat{g}_{0s}$ has the meaning of the corresponding excitation amplitude. It obeys the homogeneous counterpart of Eq. (14) and is normalized as follows [9]:

$$\left(\hat{g}^+_{0s}\frac{d\hat{A}}{d\omega}\hat{g}_{0s}\right)_{\omega=\omega_s} = -1, \tag{22}$$

with obvious notation.

For excitation probabilities, it is more convenient to use the transition density operator which is conjugated to $\hat{g}_{0s}$,

$$\hat{\rho}^{\rm Tr}_{0s} = \hat{A}\hat{g}_{0s}. \tag{23}$$

The explicit definition of the normal and anomalous components of $\hat{\rho}^{\rm Tr}_{0s}$ is as follows:

$$\rho^{{\rm Tr}(0)}_{0s}(\mathbf{r},\mathbf{r}') = \int \frac{d\varepsilon}{2\pi i}\delta G(\mathbf{r},\mathbf{r}';\varepsilon,\omega_s), \tag{24}$$

$$\rho^{{\rm Tr}(1,2)}_{0s}(\mathbf{r},\mathbf{r}') = \int \frac{d\varepsilon}{2\pi i}\delta F^{(1,2)}(\mathbf{r},\mathbf{r}';\varepsilon,\omega_s). \tag{25}$$

The TFFS equation for transition densities for nuclei with pairing correlations,

$$\hat{\rho}^{\rm Tr}_{0s} = \hat{A}(\omega_s)\hat{\mathcal{F}}\hat{\rho}^{\rm Tr}_{0s}, \tag{26}$$

is a complete analog of the QRPA set of equations. Therefore, we often name it the QRPA equation. The transition density is normalized owing to Eq. (22), and the transition matrix element for the excitation of the state $|s\rangle$ with the external field V_0 is given by

$$M_{0s} = \int \hat{V}_0\hat{\rho}^{\rm Tr}_{0s}(\mathbf{r})d\mathbf{r}. \tag{27}$$

III. CHARACTERISTICS OF THE 2^+_1 EXCITATIONS

The formalism described in the previous section is used to describe 2^+_1 states in two long isotopic chains of semimagic nuclei, lead and tin. We investigate both a pure surface and a pure volume version of pairing. More calculational details can be found in Ref. [14]. We use the so-called developed pairing approximation. In particular, there is no particle number projection procedure in our calculations; that is, particle number is conserved only on average, corresponding to the chosen chemical potential μ for the kind of nucleons under consideration. The accuracy of this approximation is examined in a lot of papers. For the self-consistent SHF method with the SLy4 force, it was found in a recent article [38] that the average difference between exact and approximate gap values is 0.12 MeV, the error being bigger in the vicinity of magic nuclei.

The effective pairing force of zero range we use [Eq. (12)] requires a regularization. In the present approach, we chose the cutoff energy $E_{\rm max}$ as a regulator. To quantify the sensitivity of the numerical results to the unphysical regulator, we follow the ideas of the renormalization procedure of effective field theory [16]. The effective coupling constants $f^{\xi}_{\rm ex}, h^{\xi}$ of the amplitude $\mathcal{F}^{\xi}$ (13) have to be determined for each value of the regulator $E_{\rm max}$. At the next step, each observable under consideration is calculated for several values of the regulator and then one obtains an error interval. As we limit ourselves to the lead and the tin chains, we deal with neutron pairing only. Let us first analyze neutron separation energies S_n, the quantity usually used for fixing pairing force parameters. More specifically, we consider the double mass differences,

$$D_N = \tfrac{1}{2}\big\{S_n(N) - \tfrac{1}{2}[S_n(N-1) + S_n(N+1)]\big\}, \tag{28}$$

with N even, which is very sensitive to the value of pairing gap because the approximate relation $D_N \simeq \bar{\Delta}$ takes place where $\bar{\Delta}$ is an average gap value. Let us begin from the lead chain. For each kind of pairing, we changed the cutoff energy from the "basic" value $E^{(0)}_{\rm max} = 36$ MeV used in Ref. [14] to $E^{(1)}_{\rm max} = 15$ MeV. The letter is approximately twice less of the

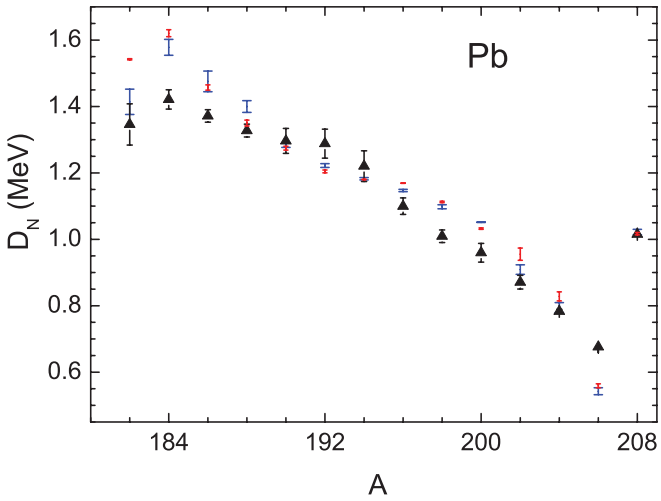

FIG. 1. (Color online) Analysis of the cutoff dependence of neutron double mass differences D_N [Eq. (28)] for lead isotopes. Black triangles with bars show the experimental D_N values taken from the mass table [39]. The red bars with narrow caps indicate the uncertainties in theoretical D_N values for surface pairing; blue bars with wide caps represent those with volume pairing.

initial cutoff value if to count from the chemical potential μ. For each value of $E_{\max}$ the pairing parameters were found to reproduce the D_N values with sufficient accuracy. In the case of the volume pairing ($h^\xi = 0$) we found $f_{\rm ex}^\xi(E_{\max})$, whereas for the surface pairing we fix the external parameter $f_{\rm ex}^\xi = -1.05$ [30] and consider the second parameter h^ξ as a free one depending on the $E_{\max}$ value. The uncertainty resulting from the fitting procedure is shown in Fig. 1 for the lead chain. For each isotope, the bar shows the difference between $D(E_{\max}^{(0)})$ and $D(E_{\max}^{(1)})$ for volume pairing (blue bars with wide caps) and surface pairing (red bars narrow with bars), correspondingly. We see that the uncertainty is rather small for each kind of pairing, often smaller than the experimental error. The average uncertainty in the double mass difference can be found according to

$$\overline{\delta D} = \sqrt{\frac{1}{N_e}\sum_{N=N_1}^{N_2}\left[D_N\left(E_{\max}^{(0)}\right) - D_N\left(E_{\max}^{(1)}\right)\right]^2}, \qquad (29)$$

with N even, $N_e = (N_2 - N_1)/2 + 1$. This quantity calculated for the surface and volume kinds of pairing is given in Table II. To estimate the corresponding inaccuracy in characteristics of the 2_1^+ states under consideration we calculated for the nucleus ^{200}Pb the difference $\delta\omega_2 = |\omega_2(E_{\max}^{(0)}) - \omega_2(E_{\max}^{(1)})|$, again for both kinds of pairing. Likewise, we studied the uncertainty of the $B(E2)$ values, $\delta B(E2, \text{up}) = |B(E2; E_{\max}^{(0)}) - B(E2; E_{\max}^{(1)})|$.

A similar analysis was made for the tin chain. The results are displayed in Fig. 2 and in the bottom part of Table II. In this case, the nucleus ^{118}Sn was chosen as a sample for calculating $\delta\omega_2$ and $\delta B(E2, \text{up})$ quantities. We see that the theoretical uncertainties under discussion in the D_N values are rather small, often less than the experimental errors. In any case, they are significantly less than the inaccuracy discussed above of the simple BCS-type theory with particle number conservation

TABLE II. Accuracy of calculation results on the cutoff parameter $E_{\max}$. Quantities $\overline{\delta D}$, $\delta\omega_2$, and $\delta B(E2, \text{up})$ are defined in the text.

Version	$\overline{\delta D}$ (MeV)	$\delta\omega_2$ (MeV)	$\delta B(E2, \text{up})(\text{e}^2\text{b}^2)$
		Pb	
Surface	0.027	0.104	0.003
Volume	0.016	0.005	0.005
		Sn	
Surface	0.016	0.022	0.004
Volume	0.045	0.052	0.006

on average. As to the characteristics of the 2_1^+ excitations, corresponding uncertainties are also moderate. Indeed, they should be compared with typical values of $\omega_2 \simeq 1$ MeV and $B(E2, \text{up}) \simeq 0.2\text{e}^2\,\text{b}^2$.

As calculations of characteristics of the 2_1^+ excitations are time consuming, for systematic calculations we employ one cutoff value $E_{\max}^{(0)} = 36$ MeV, keeping in mind the accuracy of the predictions of the theory given in Table II. For finding the parameters of the pairing force (13) we use the strategy of "soft" variation to obtain better values of S_n for both chains under consideration. Values of S_n for both kinds of pairing are compared with the data in Figs. 3 and 4. In agreement with the previous analysis of theoretical uncertainties in values of S_n (they, evidently, being the same as for D_N), we do not show them in these two figures. In the major part of the points, they just would be undistinguishable graphically. Explicit values of the pairing parameters are given in the figure captions. Remember that we use the two-parameter version of Eq. (13), with $f_\nabla^\xi = 0$. For the volume pairing ($h^\xi = 0$), one parameter remains which is smaller for lead than for tin approximately at 6%. For the surface pairing we deal with a two-parameter form of $\mathcal{F}^\xi$. The "external" pairing parameter $f_{\rm ex}^\xi$ is taken to be A independent, in accordance with its

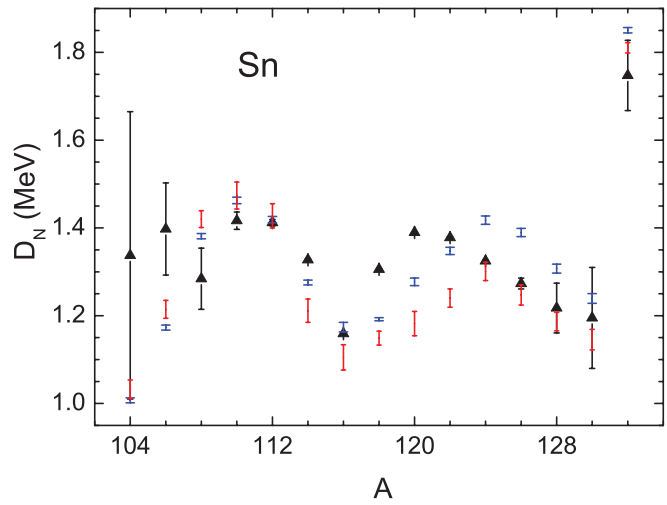

FIG. 2. (Color online) Analysis of the cutoff dependence of neutron double mass differences D_N [Eq. (28)] for tin isotopes. Black triangles with bars show the experimental D_N values taken from the mass table [39]. The red bars with narrow caps indicate the uncertainties in theoretical D_N values for surface pairing; blue bars with wide caps represent those for volume pairing.

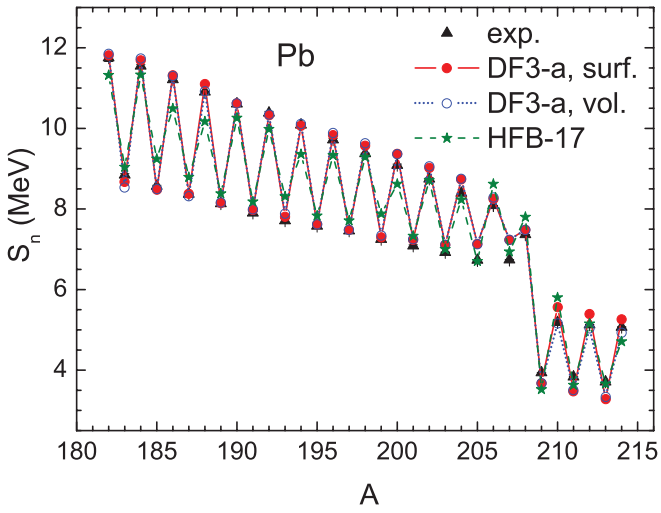

FIG. 3. (Color online) Neutron separation energies S_n for lead isotopes. The volume pairing corresponds to ($f_{\rm ex}^{\xi} = -0.31; h^{\xi} = 0$); the surface one to ($f_{\rm ex}^{\xi} = -1.05; h^{\xi} = 0.94$). The HFB theory predictions with the HFB-17 Skyrme functional are taken from Ref. [40]; experimental data from Ref. [39].

physical meaning as the free NN T matrix taken at negative energy $E = 2\mu$ [18]. As to the second one, h^{ξ}, it increases from the Sn chain to the Pb one at 2%, the resulting pairing attraction again becoming weaker, but only a little. Thus, the A independence of the pairing parameters in the case of surface pairing is weaker than for the volume one. This finding seems to favor surface pairing. As we see, the difference between the predictions for neutron separation energies is small for both versions and agreement with the experimental data is nearly perfect. For comparison, we display the predictions of the HFB-17 version of the Skyrme force [36] which has a record accuracy in overall description of nuclear masses. We see that for these two chains our accuracy in description

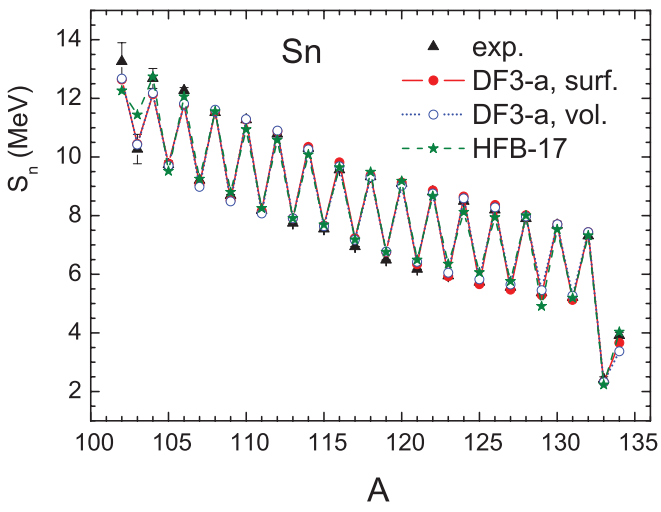

FIG. 4. (Color online) Neutron separation energies S_n for tin isotopes. The volume pairing corresponds to ($f_{\rm ex}^{\xi} = -0.33; h^{\xi} = 0$); the surface one to ($f_{\rm ex}^{\xi} = -1.05; h^{\xi} = 0.92$). The HFB theory predictions with the HFB-17 Skyrme functional are taken from Ref. [40]; experimental data from Ref. [39].

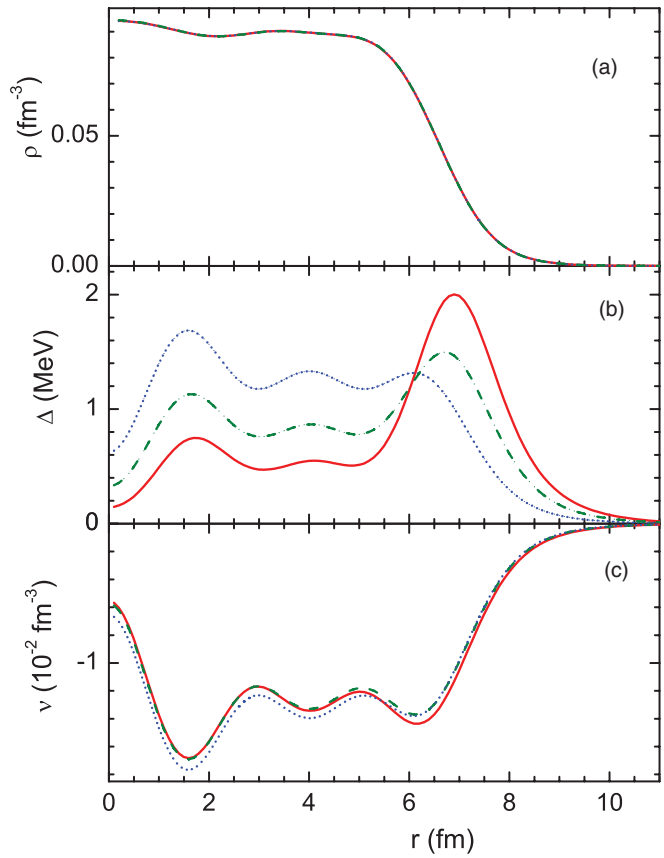

FIG. 5. (Color online) Neutron density (a), gap (b), and anomalous density (c) in ^{200}Pb nucleus. Solid red lines correspond to surface pairing; dotted blue lines correspond to volume one. Green dashes show the medium version ($f_{\rm ex}^{\xi} = -0.70; h^{\xi} = 0.50$).

of neutron separation energies is even better. Of course, we achieved the agreement by a small variation of one of two paring parameters, whereas calculations [36] are carried out with a universal set of parameters. However, the pairing part of the HFB-17 functional contains five parameters.

Figure 5 demonstrates that the normal neutron density $\rho_n(r)$ and the anomalous one, $\nu_n(r)$, both are practically insensitive to the kind of paring used in the calculation. On the contrary, the gap itself is very sensitive. For comparison, we took also a "medium" version, with ($f_{\rm ex}^{\xi} = -0.70; h^{\xi} = 0.50$). It gives S_n value approximately with the same accuracy as the previous two.

Let us now examine to what extent predictions for characteristics of 2_1^+ states are different for these two versions of pairing force which are equivalent in describing the S_n values. A comment should be made before presenting results of the QRPA calculations. Our QRPA code does not include the spin-orbit (9) and spin (11) terms of the effective interaction; therefore, the self-consistency is not complete and the excitation energy of the ghost 1^- state does not automatically vanish. In the present investigation, we fine tuned the parameter a_+^{ν} in Eq. (3) to decouple the ghost state. This change is different for different nuclei but on average the value of $|a_+^{\nu}|$ increases at $\simeq$3% in comparison with that given in Table I.

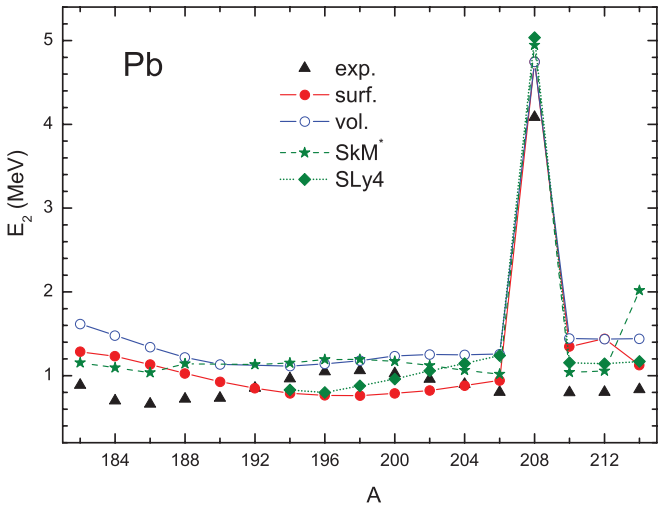

FIG. 6. (Color online) Excitation energies $\omega(2_1^+)$ for lead isotopes. Predictions for mean-field approach with the forces SkM* (dashed green line) and SLy4 (dotted green line) are taken from Ref. [27]. The EDF results are given by the solid lines.

Let us begin with the lead chain. Excitation energies ω_2 are displayed in Fig. 6 and the probabilities $B(E2, \text{up})$ in Fig. 7. Just as in Figs. 3 and 4, we do not show the theoretical uncertainties presented in Table II. Indeed, even the biggest of them, $\delta\omega_2$ value for surface pairing, can hardly be distinguishable in Fig. 6. Experimental data for both quantities are taken from Ref. [41]. For comparison, results of the QRPA calculations of Ref. [27] with the SkM* and SLy4 force are shown. Note that they were carried out with density-independent pairing. We see that the difference $\Delta\omega_2 = \omega_2^{\text{vol}} - \omega_2^{\text{surf}}$ is always positive, with the exception of the ^{210,212}Pb isotopes for which the two versions practically coincide. If we limit ourselves to isotopes $^{182–204}$Pb with developed pairing, we find $\overline{\Delta\omega_2} = 0.30$ MeV for the average value of the difference between predictions of two kinds of pairing, which is significantly bigger of the uncertainty $\delta\omega_2$ in Table II. Thus, the effect under discussion is noticeable

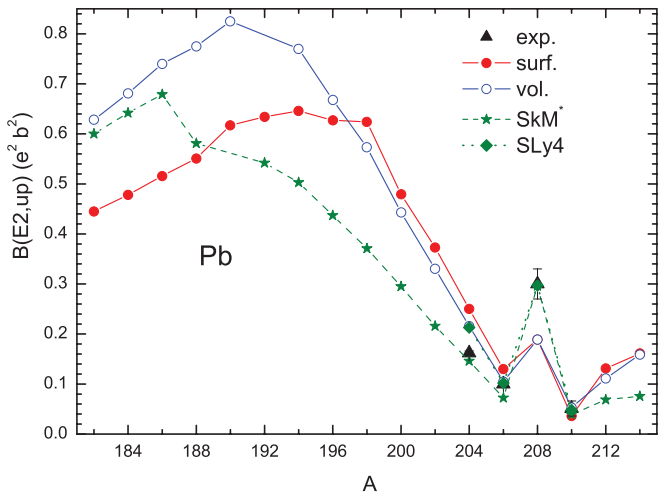

FIG. 7. (Color online) $B(E2, \text{up})$ values for lead isotopes. Predictions for the SkM* and SLy4 force are taken from Ref. [27].

for the excitation energy. Agreement with the data looks reasonable for both the versions and a little better for surface pairing. The root-mean-squared deviation of the theory from experiment is $(\Delta\omega_2)_{\text{rms}} = 0.33$ MeV for the surface pairing and $(\Delta\omega_2)_{\text{rms}} = 0.47$ MeV in volume case. Predictions of both the SkM* and SLy4 QRPA calculations for ω_2 values have approximately the same accuracy as ours.

For excitation probabilities the situation is more complex. For isotopes heavier than ^{198}Pb our "surface" and "volume" curves are very close to each other. For a lighter part of the chain the volume pairing generates larger probabilities than surface pairing does, producing differences of up to $\simeq$30%. Comparing with Fig. 6, we see that there is some unusual correlation between excitations energies and probabilities. Indeed, in magic nuclei where the pairing is absent for low-lying collective excitations there is a rule that a lower energy implies a larger probability. It can be qualitatively explained with the hydrodynamical Bohr-Mottelson (BM) model [42] which gives a simple relation for the transition density of a L vibration:

$$\rho_L^{\text{Tr,BM}} = \alpha_L \frac{d\rho}{dr}, \tag{30}$$

where $\alpha_L = 1/\sqrt{2\omega_L B_L}$ and B_L is the collective mass parameter of the BM model proportional to the nuclear mass. Then one obtains

$$B(EL, \text{up}) = \frac{2L+1}{2\omega_L B_L}(M_L)^2, \tag{31}$$

where $M_L^{\text{BM}} = (3Ze/4\pi)R^{L-1}$, with R being the nuclear radius. Thus, in the BM model a lower value of the excitation energy ω_L inevitably leads to a higher value of the excitation probability. In our calculations, the situation is opposite. In principle, this is not strange. Indeed, even in magic nuclei the BM model works only qualitatively [8]. If one solves equations of the self-consistent TFFS or any HF + RPA equations for nuclei without pairing, Eq. (30) remains approximately true, but the mass parameter becomes ω dependent and deviates from the BM model prescription significantly [8]. In nuclei with pairing, the situation becomes even more different from this simplest model as the normal component of the transition density (24) depends now from the anomalous transition amplitudes $g_{0s}^{(1,2)}$ [see Eq. (26)]. They strongly depend on the kind of pairing. As a result, the correlation between the ω_L and $B(EL)$ values of the BM type (31) can be destroyed.

Experimental probabilities are known only for four even $^{204–210}$Pb isotopes. For all of them, the SkM* and SLy4 calculations are in perfect agreement with the data. Agreement of our calculations is poorer. It is especially true for the magic ^{208}Pb nucleus where there is no pairing. It should be noted that in this nucleus the collectivity of the 2_1^+ state is not high: The $B(E2)$ value is only about 8 single-particle units (spu). For a comparison, the $B(E3)$ value for the 3_1^- state exceeds 30 spu. However, for excitations with low collectivity in nuclei without pairing the RPA solution depends strongly on the single-particle spectrum, and even a small inaccuracy in the positions of single-particle levels can change results significantly. In any case, some modification of the normal part

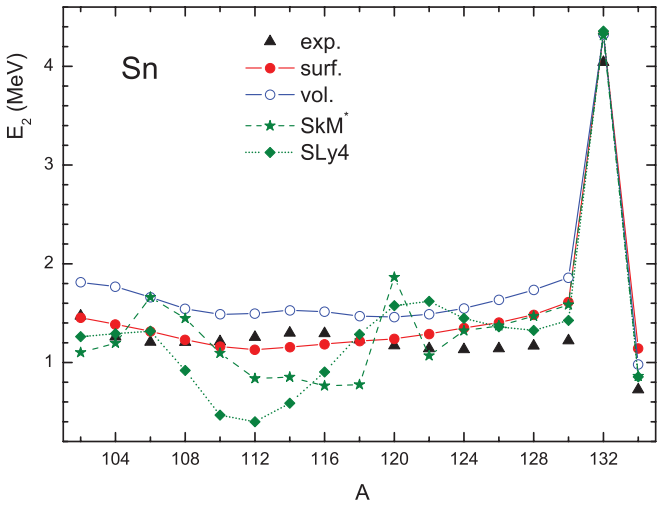

FIG. 8. (Color online) Excitation energies $\omega(2_1^+)$ for tin isotopes. Predictions for the SkM* and SLy4 force are taken from Ref. [27].

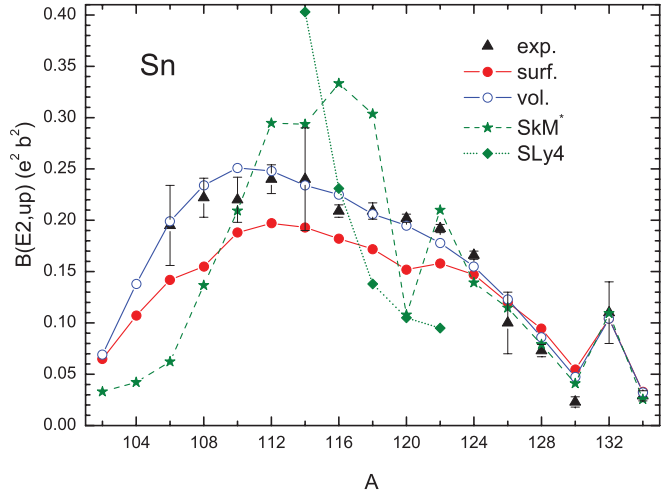

FIG. 9. (Color online) $B(E2, \text{up})$ values for tin isotopes. Predictions for the SkM* and SLy4 force are taken from Ref. [27]. Experimental data are taken for $^{114-124}$Sn from Ref. [41], for $^{126-134}$Sn from Ref. [43], and for $^{106-112}$Sn from Ref. [44–46].

of the functional DF3-a is necessary to obtain better agreement for the ^{208}Pb nucleus.

In the tin chain (see Fig. 8), the situation with the excitation spectrum is partially similar to the one in lead. Again, 2_1^+ levels are systematically higher for volume pairing than in the surface case. If we again limit ourselves to isotopes with developed pairing, $^{104-128}$Sn, we find the average difference $\overline{\Delta\omega_2} = 0.29$ MeV, very close to the corresponding value for lead. The surface predictions are now essentially closer to the experimental data. Now we have $(\Delta\omega_2)_{\text{rms}} = 0.16$ MeV for the surface pairing and $(\Delta\omega_2)_{\text{rms}} = 0.37$ MeV for the volume one. As to the SkM* spectrum, for isotopes heavier than ^{122}Sn it practically coincides with our "surface" one, both being higher than the experimental spectrum by approximately 200–300 keV. For lighter isotopes, it deviates from our surface spectrum significantly in an irregular way, whereas the latter practically coincides with the experiment in this A region. As to the SLy4 spectrum, it also looks reasonable for the heavy part of the chain but for isotopes lighter of ^{124}Sn it strongly oscillates around the experimental curve. In the dip minimum for ^{112}Sn the ω_2 value is less than the experimental one at approximately 1 MeV and it is close to an instability.

The excitation probabilities are displayed in Fig. 9. Here the results show a very complex pattern. For the heavier part of the chain, beginning at the ^{124}Sn nucleus, our two theoretical curves and the SkM* practically coincide, all being close to the experiment. The SkM* curve behaves in a nonregular way with strong deviations from the experimental data, up to $\simeq$50%–100%. The Sly4 interaction produces excitation probabilities which strongly decrease with the nucleon number A, implying drastic deviations from the data. The density functional approach is able to describe the A dependence of the experimental $B(E2, \text{up})$ values rather well. For lighter tin isotopes, our two curves began to deviate from each other, the volume one being higher by $\simeq$25%–30%, and a first glance may suggest that the volume-pairing interaction performs much better. However, one has to notice the large error bars of the experimental data in the mass region below $A = 114$.

To investigate the role of pairing itself and of the type of its density dependence in detail, let us analyze different components of the transition amplitude. Let us begin from the anomalous terms $g^{(1,2)}$ (the index "0s" is omitted for brevity). They are displayed in Fig. 10 for the ^{200}Pb nucleus. We see first that, for both the versions, the $g^{(1)}$ amplitude value is much bigger than $|g^{(2)}|$. Second, the coordinate dependence of the main $g^{(1)}$ amplitude is absolutely different for the two versions under comparison. In the surface-pairing case, a strong surface maximum dominates, whereas in the volume case $g^{(1)}$ is spread over the volume, with rather strong oscillations. In addition, it is seen that the integral effect of $g^{(1)}_{\text{surf}}$ should be noticeably bigger than that of $g^{(1)}_{\text{vol}}$. All this shows some asymmetry for

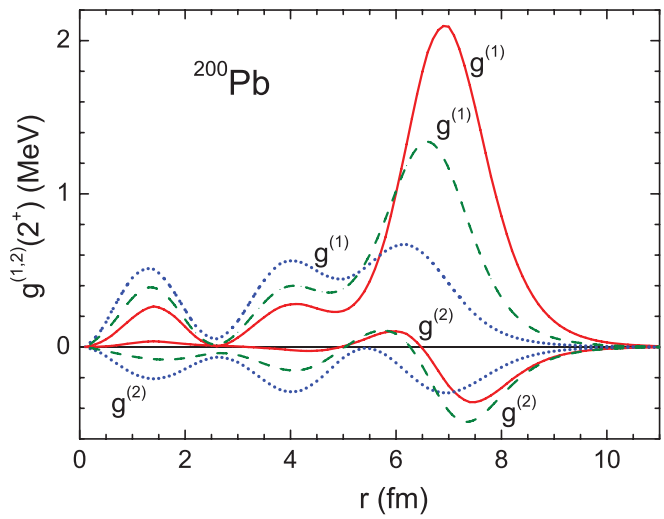

FIG. 10. (Color online) The neutron anomalous transition amplitudes $g^{(1,2)}$ in ^{200}Pb nucleus. Solid red lines correspond to surface pairing, dotted blue lines to volume pairing, and dashed green lines to a medium version of pairing ($f^{\xi}_{\text{ex}} = -0.70; h^{\xi} = 0.50$).

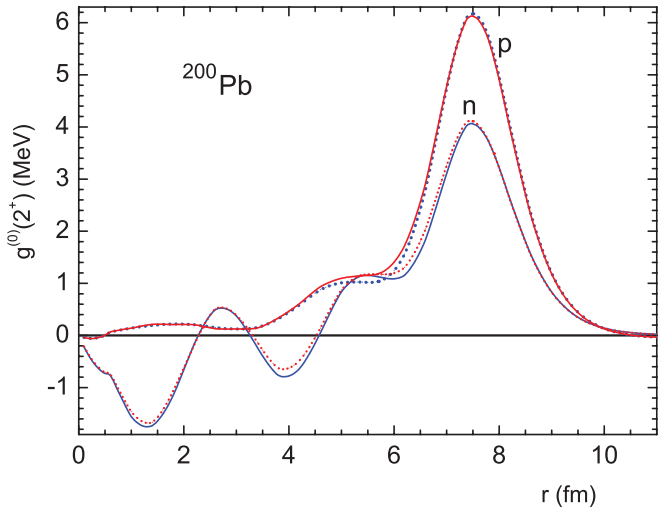

FIG. 11. (Color online) The proton and neutron normal transition amplitudes $g^{(0)}$ in ^{200}Pb nucleus. For protons, solid (red) line corresponds to surface pairing and dotted (blue) one, to volume pairing. For neutrons, solid (blue) line corresponds to volume pairing and dotted (red) one, to surface pairing.

Bogolyubov quasiparticles and quasiholes. Such a situation is typical for nuclei which are close to the magic core.

The normal proton and neutron amplitudes $g^{(0)}$ for the same nucleus are displayed in Fig. 11. As we see, for this quantity the influence of the kind of pairing used is minimal. Thus, evidently, the rather big value of the difference $\Delta\omega_2 \simeq 300$ keV for this nucleus is explained with different contributions of the anomalous amplitude $g^{(1)}$, which is much stronger in the case of surface pairing. For the transition densities (see Fig. 12), the effect is rather small but a little bigger than for the normal amplitudes $g^{(0)}$. This additional enhancement of the surface maximum of $\rho^{Tr(0)}(r)$ in the surface-pairing case again originates from the term with $g^{(1)}$ in Eq. (23). In its turn, it explains the increase of the $B(E2)$ value in this nucleus for the surface case.

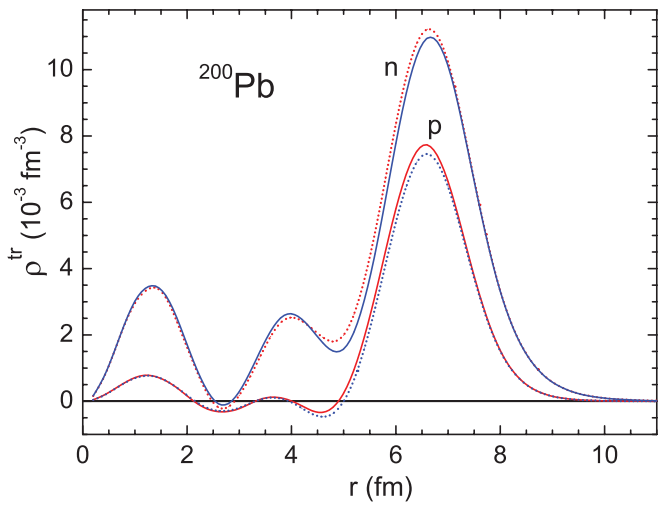

FIG. 12. (Color online) The proton and neutron transition densities $\rho^{Tr(0)}$ in ^{200}Pb nucleus. Red solid and dotted lines correspond to surface pairing, blue ones to volume pairing.

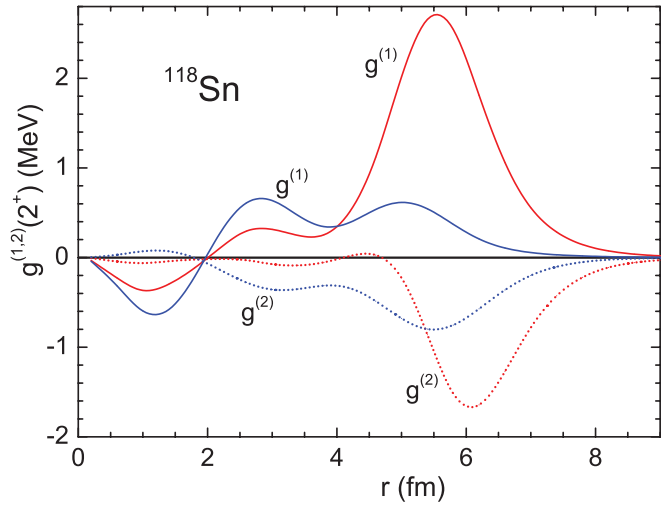

FIG. 13. (Color online) The neutron anomalous transition amplitudes $g^{(1,2)}$ in ^{118}Sn nucleus. Red solid and dotted lines correspond to surface pairing, blue ones to volume pairing.

Let us go to the tin chain. Figs. 13– 15 present for the ^{118}Sn nucleus the same quantities which were displayed in Figs. 10–12 for the ^{200}Pb nucleus. This nucleus is in the middle of the chain, and all properties of the "developed" pairing, in particular, particle-hole symmetry should take place. Indeed, now (see Fig. 13) the amplitudes $g^{(1)}$ and $g^{(2)}$ possess a similar form and absolute value and are of the opposite sign. In the result, we have $|g^{(-)} = g^{(1)} - g^{(2)}| \gg |g^{(+)} = g^{(1)} + g^{(2)}|$, as it should be [9]. Again, as in the ^{200}Pb case, the effect of the kind of pairing on the magnitude of $g^{(1,2)}$ is drastic. As to that for the normal amplitudes $g^{(0)}$ and transition densities $\rho^{Tr(0)}$, again it is rather moderate but of the another sign. Now in the volume case, the surface peaks in both these quantities are higher and, correspondingly, the $B(E2)$ value is bigger. Evidently, in this case we deal with some destructive

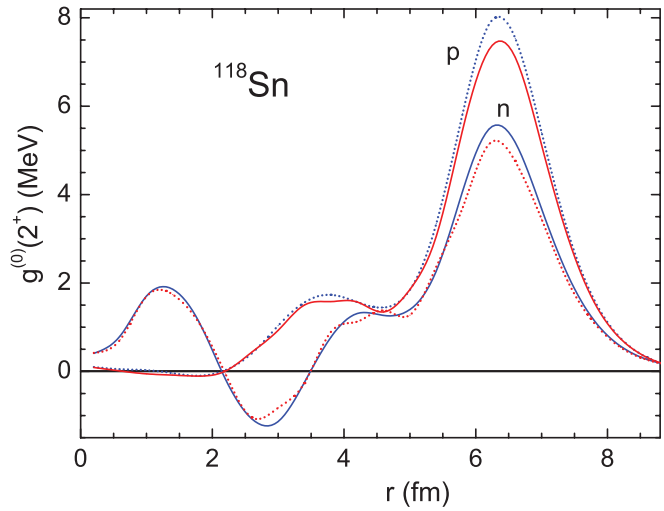

FIG. 14. (Color online) The proton and neutron normal transition amplitudes $g^{(0)}$ in ^{118}Sn nucleus. Red solid and dotted lines correspond to surface pairing, blue ones to volume pairing.

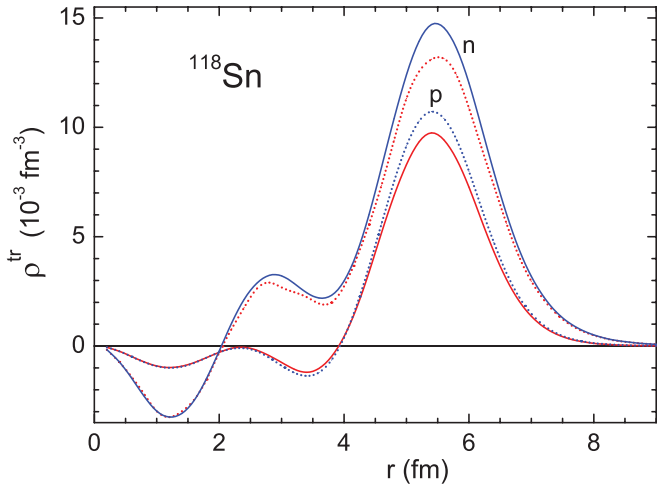

FIG. 15. (Color online) The proton and neutron transition densities $\rho^{Tr(0)}$ in ^{118}Sn nucleus. Red solid and dotted lines correspond to surface pairing, blue ones to volume pairing.

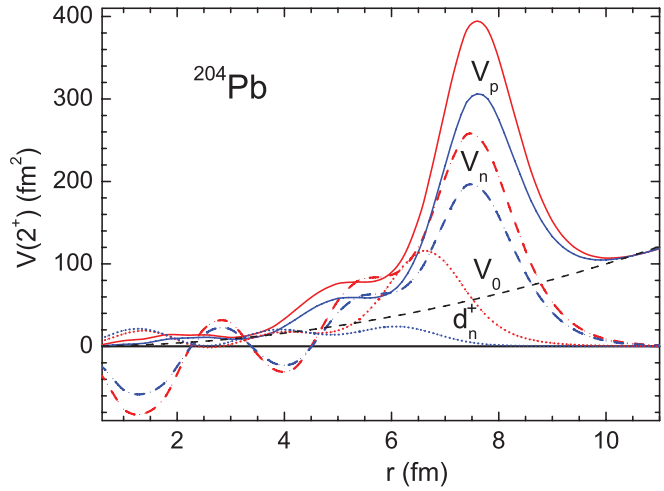

FIG. 17. (Color online) Static effective fields V_p (solid lines), V_n (dashes), and d_n^+ (dots) in ^{204}Pb nucleus. Red lines correspond to surface pairing, blue ones to volume pairing.

interference between normal and anomalous contributions to solutions of the equations of Sec. II.

To summarize, we see an effect of the type of pairing on the characteristics of the 2_1^+ states in spherical nuclei. The excitation energies ω_2 are systematically lower in the surface case to $\Delta\omega_2 \simeq 300$ keV, and the surface values are, as a rule, closer to the data. For $B(E2)$ values, the effect is not so regular and here the volume version predictions on average look better. Thus, the present analysis is compatible with both volume and surface pairing.

In conclusion of this section we compare in Fig. 16 the charge transition density $\rho_{ch}^{Tr}(r)$ in the ^{118}Sn nucleus with the experimental transition charge density found with a model independent analysis of the elastic electron scattering in Ref. [47]. The theoretical charge density is obtained from $\rho_p^{Tr}(r)$ and $\rho_n^{Tr}(r)$ functions displayed in Fig. 13, taking into account relativistic corrections [48]. For both versions of pairing the agreement with the data is quite reasonable, and it is a little better in the surface case.

IV. QUADRUPOLE MOMENTS OF ODD NUCLEI

Recently, magnetic moments of odd spherical nuclei have been calculated [49,50] within the same self-consistent approach as the one used here. A reasonable description of the data for more than 100 of the spherical nuclei was obtained. Especially high accuracy was reached for semimagic nuclei considered in the "single-quasiparticle approximation" where one quasiparticle in the fixed state $\lambda = (n, l, j, m)$ with the energy ε_λ is added to the even-even core. According to the TFFS, a quasiparticle differs from a particle of the single-particle model in two respects. First, it possesses the local charge e_q (in our case, we have $e_q^p = 1$, $e_q^n = 0$), and, second, the core is polarized owing to the interaction between

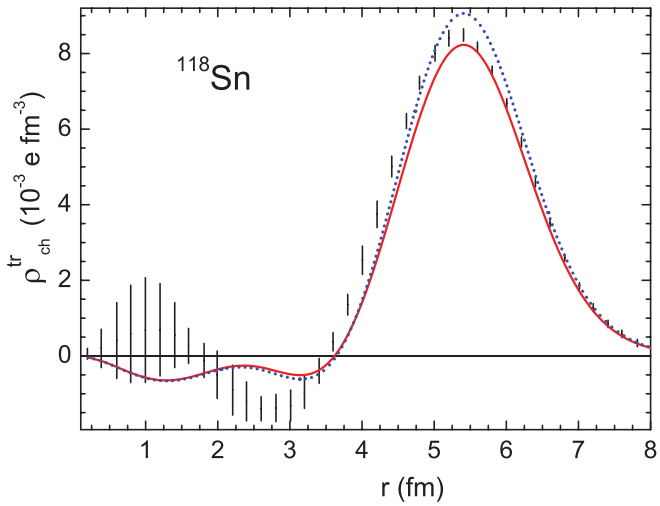

FIG. 16. (Color online) The charge transition densities $\rho_{ch}^{Tr(0)}$ in ^{118}Sn nucleus. The solid red line corresponds to surface pairing, the dotted blue one to volume pairing.

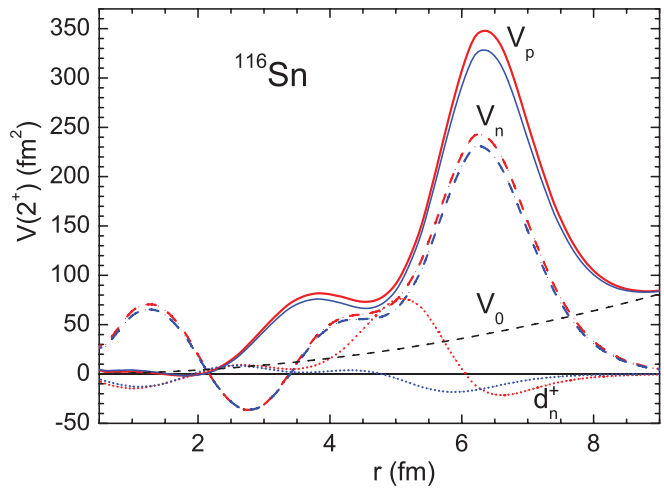

FIG. 18. (Color online) Static effective fields V_p (solid lines), V_n (dashes), and d_n^+ (dots) in ^{116}Sn nucleus. Red lines correspond to surface pairing, blue ones to volume pairing.

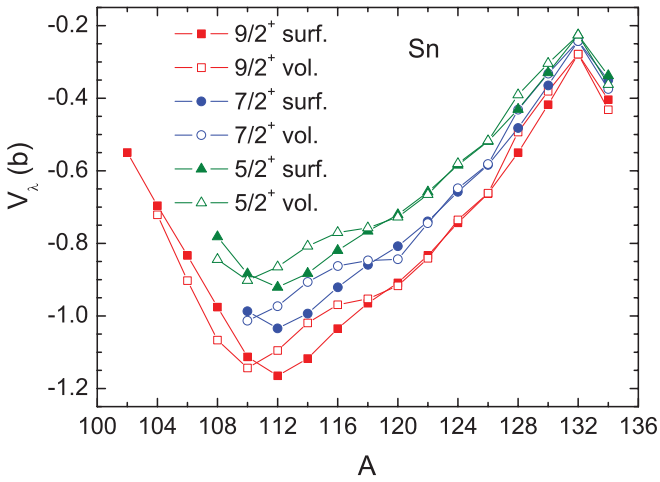

FIG. 19. (Color online) Diagonal matrix elements V_λ^p of the effective proton quadrupole field in the tin isotopes. Solid symbols correspond to surface pairing, open ones to volume pairing.

the particle and the core nucleons via the LM amplitude. In other words, the quasiparticle possesses the effective charge $e_{\rm eff}$ caused by the polarizability of the core which is found by solving the above TFFS equations. In the many-particle shell model [51,52], a similar quantity is introduced as a phenomenological parameter which describes polarizability of the core consisting of outside nucleons.

In nonmagic nuclei, the term quasiparticle takes a double meaning. In addition to the initial LM concept we consider the Bogolyubov quasiparticles with occupation numbers $n_\lambda^{\rm B} = (E_\lambda - \varepsilon_\lambda)/2E_\lambda$ and energies $E_\lambda = \sqrt{(\varepsilon_\lambda - \mu)^2 + \Delta_\lambda^2}$ and solve the set of the QRPA equations (14) instead of one RPA equation.

The success of the single-quasiparticle approximation in describing the magnetic moments of semimagic nuclei makes it of interest to try to use the same approach for quadrupole moments. In this article, we do such analysis limiting ourselves to odd neighbors of the even tin and lead isotopes considered in the previous section. To our knowledge, there is no systematic calculation of quadrupole moments of these nuclei.

The static quadrupole moment of an odd nucleus in the single-particle state λ can be found in terms of the effective field (14) with the static external field $V_0 = \sqrt{16\pi/5}r^2 Y_{20}(\theta)$ as follows [9,53]:

$$Q_\lambda^{p,n} = \left(u_\lambda^2 - v_\lambda^2\right) V_\lambda^{p,n}, \tag{32}$$

where u_λ, v_λ are the Bogolyubov coefficients and

$$V_\lambda = -\frac{2j-1}{2j+2}\int V(r) R_{nlj}^2(r) r^2 dr. \tag{33}$$

The j-dependent factor in Eq. (33) appears owing to the angular integral [54]. For $j > 1/2$ it is always negative. For odd neighbors of a magic nucleus the "Bogolyubov" factor in Eq. (32) reduces to 1 for a particle state and to -1 for a hole one.

Components of the static effective field $\hat{V}(\omega = 0)$, that is $V^{n,p}(r)$ and $d_n^+(r) = d_n^{(1)}(r) + d_n^{(2)}(r)$, are displayed in Figs. 17 and 18 for ^{204}Pb and ^{116}Sn nuclei, correspondingly. Note that the identity $d^-(\omega = 0) = 0$ takes place [9]. One can see large surface maxima of the quantities $V^{n,p}(r)$ similar to

TABLE III. Quadrupole moments Q(eb) of odd-proton nuclei.

Nucleus	λ_0	$Q_{\rm exp}$	$Q_{\rm th}^{\rm surf}$	$Q_{\rm th}^{\rm vol}$	Q_0	$e_{\rm eff}^{\rm surf}$	$e_{\rm eff}^{\rm vol}$
^{105}In	$1g_{9/2}$	+0.83(5)	+0.83	+0.90	+0.18	4.6	5.0
^{107}In	$1g_{9/2}$	+0.81(5)	+0.98	+1.07	+0.18	5.4	5.9
^{109}In	$1g_{9/2}$	+0.84(3)	+1.11	+1.14	+0.18	6.2	6.3
^{111}In	$1g_{9/2}$	+0.80(2)	+1.16	+1.10	+0.19	6.1	5.8
^{113}In	$1g_{9/2}$	+0.80(4)	+1.12	+1.02	+0.19	5.9	5.4
^{115}In	$1g_{9/2}$	+0.81(5), 0.58(9)	+1.03	+0.97	+0.19	5.4	5.1
^{117}In	$1g_{9/2}$	+0.829(10)	+0.96	+0.95	+0.19	5.1	5.0
^{119}In	$1g_{9/2}$	+0.854(7)	+0.91	+0.92	+0.19	4.8	4.8
^{121}In	$1g_{9/2}$	+0.814(11)	+0.83	+0.84	+0.19	4.4	4.4
^{123}In	$1g_{9/2}$	+0.757(9)	+0.74	+0.74	+0.19	3.9	3.9
^{125}In	$1g_{9/2}$	+0.71(4)	+0.66	+0.74	+0.19	3.8	3.9
^{127}In	$1g_{9/2}$	+0.59(3)	+0.55	+0.49	+0.19	2.9	2.6
^{115}Sb	$2d_{5/2}$	−0.36(6)	−0.88	−0.81	−0.14	6.3	5.8
^{117}Sb	$2d_{5/2}$	−0(2)	−0.82	−0.77	−0.14	5.9	5.5
^{119}Sb	$2d_{5/2}$	−0.37(6)	−0.77	−0.76	−0.14	5.5	5.4
^{121}Sb	$2d_{5/2}$	−0.36(4), −0.45(3)	−0.72	−0.73	−0.14	5.1	5.2
	$1g_{7/2}^*$	−0.48(5)	−0.81	−0.81	−0.17	4.8	4.8
^{123}Sb	$1g_{7/2}$	−0.49(5)	−0.74	−0.74	−0.17	4.4	4.4
^{205}Tl	$3d_{3/2}^*$	0.74(15)	+0.23	+0.23	+0.12	1.9	1.9
^{203}Bi	$1h_{9/2}$	−0.68(6)	−1.32	−0.91	−0.25	5.3	3.6
^{205}Bi	$1h_{9/2}$	−0.59(4)	−0.94	−0.72	−0.25	3.8	2.9
^{209}Bi	$1h_{9/2}$	−0.37(3), −0.55(1) −0.77(1), −0.40(5)	−0.34	−0.34	−0.25	1.4	1.4

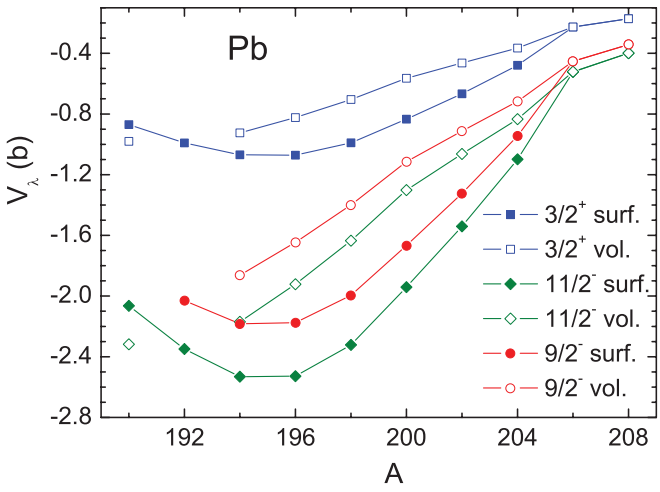

FIG. 20. (Color online) Diagonal matrix elements V_λ^p of the effective proton quadrupole field in the lead isotopes. Solid symbols correspond to surface pairing, open ones to volume pairing.

those in Figs. 11 and 14 for the BM-like transition amplitudes $g^{(0)}_{n,p}(r)$. In-volume ("quantum") corrections are relatively small; therefore the integral in Eq. (33) is always positive. For protons, it is noticeably larger than the similar integral with the bare field V^0; see the discussion on the effective charges below.

Diagonal matrix elements (33) of the proton effective field are displayed in Fig. 19 for the tin isotopes and in Fig. 20 for the lead ones. As is seen, for a major part of the tin isotopes, the difference between values of proton matrix elements V_λ^p surface and volume pairing is quite small. Only for $^{112-116}$Sn nuclei it reaches 10%. In the lead region, the difference is more pronounced, reaching $\simeq$30%–40% for $9/2^-$ and $11/2^-$ states.

TABLE IV. Quadrupole moments Q(eb) of odd-neutron nuclei.

Nucleus	λ_0	$Q_{\rm exp}$	$Q_{\rm th}^{\rm surf}$	$Q_{\rm th}^{\rm vol}$	$e_{\rm eff}^{\rm surf}$	$e_{\rm eff}^{\rm vol}$
^{109}Sn	$2d_{5/2}$	+0.31(10)	+0.25	+0.27	3.5	3.7
^{111}Sn	$1g_{7/2}$	+0.18(9)	+0.05	+0.10	4.0	3.9
^{113}Sn	$1h^*_{11/2}$	0.41(4), 0.48(5)	−0.78	−0.75	4.4	4.1
^{115}Sn	$1g^*_{7/2}$	0.26(3)	+0.38	+0.38	3.9	3.6
	$1h^*_{11/2}$	0.38(6)	−0.70	−0.67	4.2	3.8
^{117}Sn	$1h^*_{11/2}$	−0.42(5)	−0.59	−0.58	3.9	3.7
^{119}Sn	$2d^*_{3/2}$	+0.094(11), −0.065(5), −0.061(3)	−0.03	−0.02	3.0	2.9
	$1h^*_{11/2}$	0.21(2)	−0.46	−0.45	3.6	3.5
^{121}Sn	$2d_{3/2}$	−0.02(2)	+0.06	+0.08	2.9	2.9
	$1h^*_{11/2}$	−0.14(3)	−0.29	−0.29	3.3	3.3
^{123}Sn	$1h_{11/2}$	+0.03(4)	−0.12	−0.10	3.0	2.9
^{125}Sn	$1h_{11/2}$	+0.1(2)	+0.04	+0.06	2.7	2.7
^{191}Pb	$1i^*_{13/2}$	+0.085(5)	+0.0004	+0.10	5.3	5.9
^{193}Pb	$1i^*_{13/2}$	+0.195(10)	+0.33	+0.39	6.5	5.5
^{195}Pb	$1i^*_{13/2}$	+0.306(15)	+0.69	+0.66	6.6	5.2
^{197}Pb	$3p_{3/2}$	−0.08(17)	+0.19	+0.14	5.2	3.8
	$1i^*_{13/2}$	+0.38(2)	+0.98	+0.78	6.4	4.6
^{199}Pb	$3p_{3/2}$	+0.08(9)	+0.27	+0.19	4.5	3.1
^{201}Pb	$2f_{5/2}$	−0.01(4)	+0.14	+0.09	4.2	2.8
^{203}Pb	$2f_{5/2}$	+0.10(5)	+0.28	+0.22	3.2	2.3
^{205}Pb	$2f_{5/2}$	+0.23(4)	+0.34	+0.28	2.6	2.0
	$1i^*_{13/2}$	0.30(5)	+0.67	+0.56	3.0	2.2
^{209}Pb	$2g_{9/2}$	−0.3(2)	−0.26	−0.26	0.9	0.9

Corresponding quadrupole moments for nuclei with odd proton number $Z = 50 \pm 1$ and $Z = 82 \pm 1$ are presented in Table III. As is noted above, in this case the Bogolyubov factor in Eq. (32) is trivial, equal to ± 1. To check our approach, we selected only nuclei where there are experimental data and those which satisfy presumably the single-quasiparticle approximation. In particular, we excluded several light Tl isotopes with known quadrupole moments of low-lying excited $9/2^-$ states. If to suppose that they are single-quasiparticle $1h_{9/2}$ states, they should have essentially higher excitation energies than they do.

Experimental data are taken from the compilation [55]. From several cases of proton excited isomeric states we limit ourselves with only two, the $1g^*_{7/2}$ state in the ^{121}Sb and $2d^*_{3/2}$ state in ^{205}Tl nuclei, for which the hypothesis on the single-quasiparticle structure seems to us more or less safe. Again, we presented results for both the kinds of nuclear pairing (the quantities $Q_{\rm th}^{\rm surf}$ and $Q_{\rm th}^{\rm vol}$ for surface and volume pairing, correspondingly). In the sixth column of the table, the single-particle quadrupole moment Q_0 is presented, which is found from Eqs. (32) and (33) with substitution $V \to V_0$. As follows from Fig. 17, for odd-proton neighbors of the tin isotopes, difference between values of quadrupole moments for surface and volume pairing is quite small, in limits of 10%. In the lead region (see Fig. 20), the difference is more pronounced, but here the number of the data is very small, only 4. In addition, only in the ^{203,205}Bi and ^{205}Tl case neutron pairing exists. For these nuclei, the effect under discussion reaches $\simeq$30%–40%.

For the long chain of 12 In isotopes agreement with the data is quite reasonable. For five Sb isotopes (six values of the quadrupole moment) agreement is rather poor, disagreement reaching $\simeq$50%–100%. A similar situation takes place for two lighter Bi isotopes. For the ^{209}Bi isotope where pairing is absent experimental data are contradictory. We think that the main reason of existing disagreements is neglecting the phonon coupling effects.

Let us go to odd-neutron nuclei, the odd tin and lead isotopes. The results are presented in Table IV and Figs. 21 and 22. In selecting nuclei for the table, we used the same concept as for protons. In this case, we included into the analysis 12 excited states, in addition to the ground ones. With the only exception of the ^{209}Pb nucleus, all the nuclei under consideration exhibit pairing effects and the factor $(u_\lambda^2 - v_\lambda^2)$ in Eq. (32) becomes nontrivial. It changes permanently depending on the state λ and the nucleus under consideration. Note that in the case of magnetic moments the factor of $(u_\lambda^2 + v_\lambda^2) = 1$ appears in the relation analogous to Eq. (32) [53]. In our case, this factor determines the sign of the quadrupole moment. In all cases when the sign of the experimental moment is known the theoretical sign is correct. This makes it possible to use our predictions to determine the sign when it is unknown. The factor under discussion depends essentially on values of the single-particle basis energies ε_λ reckoned from the chemical

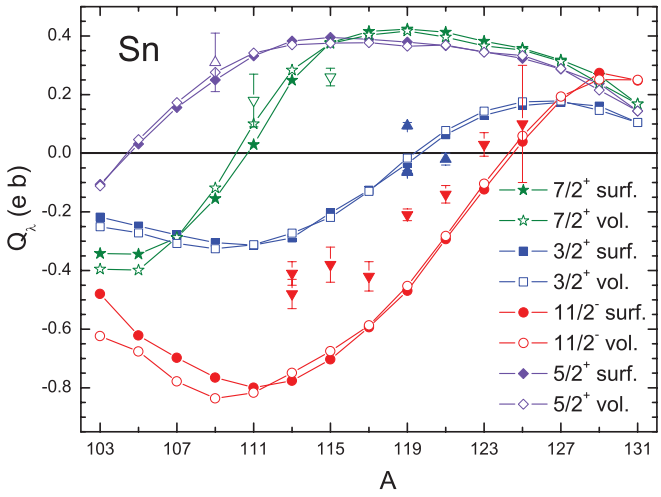

FIG. 21. (Color online) Quadrupole moments of odd tin isotopes. Solid symbols correspond to surface pairing, open ones to volume pairing. Experimental data are shown with ▲ for $3/2^+$, ▼ for $11/2^-$, ▽ for $5/2^+$, and ▽ for $7/2^+$ states.

potential μ as we have $(u_\lambda^2 - v_\lambda^2) = (\varepsilon_\lambda - \mu)/E_\lambda$. Keeping in mind such sensitivity, we found this quantity for a given odd nucleus $(Z, N+1)$, N even, taking into account the blocking effect in the pairing problem [53] putting the odd neutron to the state λ under consideration. For the V_λ value in Eq. (32) we used the half-sum of these values in two neighboring even nuclei. We consider agreement with the data reasonable if we have $|Q_{\rm th} - Q_{\rm exp}| < 0.1$–$0.2$e b. If to use such a criterion, there are 7 "bad" cases in Table IV and 16 "good." Several rather strong disagreements with the experimental data in Table IV for high j levels $1h_{11/2}$ in Sn isotopes and $1i_{13/2}$ in Pb isotopes originate just from their too distant positions from the Fermi level. Thus, the Q values depend strongly on the single-particle level structure. Again, as for protons, the difference between predictions of the two models under consideration is, as a rule,

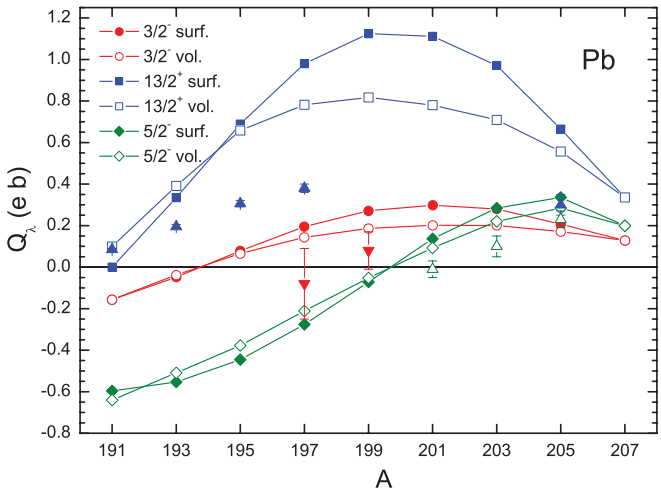

FIG. 22. (Color online) Quadrupole moments of odd lead isotopes. Solid symbols correspond to surface pairing, open ones to volume pairing. Experimental data are shown with ▲ for $13/2^+$, ▼ for $3/2^-$, and ▽ for $5/2^-$ states.

rather small, and only for $1i_{13/2}$ states in the lead chain does it reach ≃20%–30%.

In the last two columns of Tables III and IV, the effective charges are presented, which are defined as $e_{\rm eff}^{p,n} = V_\lambda^{p,n}/(V_0^p)_\lambda$. It is a direct characteristic of the core polarizability by the quadrupole external field. In these tables, there are only two nuclei, ^{209}Bi and ^{209}Pb, with a double-magic core, and in this case the polarizability is rather moderate, $e_{\rm eff}^p = 1.4$, $e_{\rm eff}^n = 0.9$. In nuclei with an unfilled neutron shell it becomes much stronger, $e_{\rm eff} \simeq 3$–6. The reason is rather obvious. Indeed, for the case of a positive parity field V_0, virtual transitions inside the unfilled shell begin to contribute and small energy denominators appear in the propagator $\mathcal{L}^n$ (18) playing the main role in the problem under consideration. It enhances the neutron response to the field V_0 and, via the strong LM neutron-proton interaction amplitude $\mathcal{F}^{np}$, the proton response as well. Results for the chain ^{203,205,209}Bi show how the polarizability grows with increase of the number of neutron holes. Keeping in mind this physics, one can represent the effective charges as $e_{\rm eff}^p = 1 + e_{\rm pol}^p$, $e_{\rm eff}^n = e_{\rm pol}^n$, where $e_{\rm pol}^{p,n}$ is the pure polarizability charge. To separate contributions of the unfilled shells and core nucleons explicitly, one can divide the Hilbert space of the QRPA equations (14) to the "valent" and subsidiary ones and carry out the corresponding renormalization procedure [56].

V. DISCUSSION AND CONCLUSIONS

The effect of the density dependence of the pairing interaction to low-lying quadrupole excitations in spherical nuclei is analyzed for two isotopic chains of semimagic nuclei. Static quadrupole moments of neighboring odd nuclei are also examined. The complete set of the QRPA-like TFFS equations for response functions is solved in a self-consistent way within the EDF approach to superfluid nuclei with previously fixed parameters of the functional. The DF3-a functional [30] is used which is a small modification of the functional DF3 [13,14]. Specifically, spin-orbit and effective tensor terms of the initial EDF DF3 were changed. Two models for effective pairing force are considered, the surface and the volume ones, which give rise to approximately the same accuracy in reproducing mass differences. A noticeable effect in excitation energies ω_2 is found: Predictions for the volume model are systematically higher than the surface ones by $\Delta\omega_2 \simeq 200$–$400$ keV. As to the excitation probabilities $B(E2, \uparrow)$, the effect is not so regular; however, as a rule, the volume values are also higher. Thus, the correlation between these two quantities typical for the BM model, where a higher frequency always results in a lower probability, is destroyed. On the average, both models reasonably agree with the data. In addition, they both reproduce rather well the model-independent charge density $\rho_{\rm ch}^{\rm Tr}(2_1^+)$ for the ^{118}Sn nucleus.

Comparison with recent QRPA calculations [27] with the Skyrme force SkM* and SLy4 shows that for the lead chain they agree with the data a little better than our results but for the tin chain the situation is opposite and our predictions occur to be essentially better. The surface model is systematically better in describing the energies ω_2, whereas the excitation

probabilities are, as a rule, reproduced better with the volume model.

Whereas the charge radii study [14] and *ab initio* theory of paring [18,24] favor the surface pairing, the $\omega(2_1^+)$ and $B(E2, \text{up})$ data do not make it possible to prefer any of the two kinds of pairing.

A reasonable agreement with experiment for the quadrupole moments of odd neighbors of the even tin and lead isotopes has been obtained for the most part of nuclei considered. For odd-proton this confirms that the single-quasiparticle approximation works sufficiently well. For odd-neutron isotopes under consideration, the validity of this approach was checked previously with the analysis of magnetic moments [50]. In the case we consider, the problem is more complicated than for odd proton isotopes as the Bogolyubov factor $(u_\lambda^2 - v_\lambda^2) = (\varepsilon_\lambda - \mu)/E_\lambda$ comes to the quadrupole moment value, in addition to the matrix element of the effective field V_λ. This factor makes the quadrupole moment value very sensitive to accuracy of calculating the single-particle energy ε_λ of the state under consideration, especially near the Fermi surface as the quantity Q_λ vanishes at $\varepsilon_\lambda = \mu$. For such a situation, the influence of the coupling of single-particle degrees of freedom with phonons (see [50,57]) should be especially important. This rather complicated problem will be considered separately.

As to the effect of the density dependence of pairing, for quadrupole moments it is, on the average, less than for quadrupole transitions. It depends on a nucleus examined and on the odd-nucleon state as well. In the tin region, it is, as a rule, of the order of $\simeq$10%. However, in the lead region it is higher and reaches $\simeq$30%–50% for ^{203,205}Bi and ^{205}Pb.

ACKNOWLEDGMENTS

We thank J. Engel and J. Terasaki for kindly supplying us with tables of the results of the QRPA calculations [27] with the SkM* and SLy4 force. Four of us, S. T., S. Ka., E. S., and D. V., are grateful to Institut für Kernphysik, Forschungszentrum Jülich for hospitality. The work was partly supported by the DFG and RFBR Grants No. 436RUS113/994/0-1 and No. 09-02-91352NNIO-a, by Grants No. NSh-7235.2010.2 and No. 2.1.1/4540 of the Russian Ministry for Science and Education, and by RFBR Grants No. 09-02-01284-a and No. 11-02-00467-a.

[1] T. Niksic, D. Vretenar, and P. Ring, Prog. Part. Nucl. Phys. **66**, 519 (2011).
[2] J. Erler *et al.*, Phys. Part. Nuclei **41**, 851 (2010).
[3] M. Bender, P.-H. Heenen, and P.-G. Reinhard, Rev. Mod. **75**, 121 (2003).
[4] W. Kohn and L. J. Sham, Phys. Rev. A **140**, 1133 (1965).
[5] R. O. Jones and O. Gunnarson, Rev. Mod. Phys. **61**, 689 (1989).
[6] L. N. Oliveira, E. K. U. Gross, and W. Kohn, Phys. Rev. Lett. **60**, 2430 (1988).
[7] D. N. Basov *et al.*, Rev. Mod. Phys. **83**, 473 (2011).
[8] V. A. Khodel and E. E. Saperstein, Phys. Rep. **92**, 183 (1982).
[9] A. B. Migdal, *Theory of finite Fermi Systems and Applications to Atomic Nuclei* (Wiley, New York, 1967).
[10] S. A. Fayans and V. A. Khodel, JETP Lett. **17**, 444 (1973).
[11] V. A. Khodel, E. E. Saperstein, and M. V. Zverev, Nucl. Phys. A **465**, 397 (1987).
[12] A. V. Smirnov, S. V. Tolokonnikov, and S. A. Fayans, Sov. J. Nucl. Phys. **48**, 995 (1988).
[13] S. A. Fayans, JETP Lett. **68**, 169 (1998).
[14] S. A. Fayans, S. V. Tolokonnikov, E. L. Trykov, and D. Zawischa, Nucl. Phys. A **676**, 49 (2000).
[15] J. Erler, P. Klüpfel, and P.-G. Reinhard, Phys. Rev. C **82**, 044307 (2010).
[16] E. Epelbaum, H.-W. Hammer, and U.-G. Meissner, Rev. Mod. Phys. **81**, 1773 (2009).
[17] J. E. Drut, R. J. Furnstahl, and L. Platter, Prog. Part. Nucl. Phys. **64**, 120 (2010).
[18] M. Baldo, U. Lombardo, E. E. Saperstein, and M. V. Zverev, Phys. Lett. B **477**, 410 (2000).
[19] M. Baldo, U. Lombardo, E. E. Saperstein, and M. V. Zverev, Phys. Rep. **391**, 261 (2004).
[20] M. Baldo, U. Lombardo, S. S. Pankratov, and E. E. Saperstein, J. Phys. G **37**, 064016 (2010).
[21] S. S. Pankratov, M. V. Zverev, M. Baldo, U. Lombardo, and E. E. Saperstein, Phys. Rev. C **84**, 014321 (2011).
[22] F. Barranco, R. A. Broglia, H. Esbensen, and E. Vigezzi, Phys. Lett. B **390**, 13 (1997).
[23] F. Barranco *et al.*, Eur. Phys. J. A **21**, 57 (2004).
[24] A. Pastore, F. Barranco, R. A. Broglia, and E. Vigezzi, Phys. Rev. C **78**, 024315 (2008).
[25] A. Bulgac and Y. Yu, Phys. Rev. Lett. **88**, 042504 (2002).
[26] Y. Yu and A. Bulgac, Phys. Rev. Lett. **90**, 222501 (2003).
[27] J. Terasaki, J. Engel, and G. F. Bertsch, Phys. Rev. C **78**, 044311 (2008).
[28] A. P. Severyukhin, V. V. Voronov, and N. V. Giai, Phys. Rev. C **77**, 024322 (2008).
[29] G. F. Bertsch, M. Girod, S. Hilaire, J.-P. Delaroche, H. Goutte, and S. Péru, Phys. Rev. Lett. **99**, 032502 (2007).
[30] S. V. Tolokonnikov and E. E. Saperstein, Phys. At. Nucl. **73**, 1684 (2010).
[31] D. J. Horen, G. R. Satchler, S. A. Fayans, and E. L. Trykov, Nucl. Phys. A **600**, 193 (1996).
[32] E. E. Saperstein and S. V. Tolokonnikov, Phys. At. Nucl. **73**, 1277 (2011).
[33] A. B. Migdal, *Theory of Finite Fermi Systems and Applications to Atomic Nuclei*, 2nd ed. [in Russian] (Nauka, Moscow, 1982).
[34] E. E. Saperstein and M. A. Troitsky, Sov. J. Nucl. Phys. **1**, 284 (1965).
[35] M. V. Zverev and E. E. Saperstein, Sov. J. Nucl. Phys. **42**, 683 (1985).
[36] S. Goriely, N. Chamel, and J. M. Pearson, Phys. Rev. Lett. **102**, 152503 (2009).
[37] S. T. Belyaev, A. V. Smirnov, S. V. Tolokonnikov, and S. A. Fayans, Sov. J. Nucl. Phys. **45**, 783 (1987).
[38] A. Mukherjee, Y. Alhassid, and G. F. Bertsch, Phys. Rev. C **83**, 014319 (2011).
[39] G. Audi, A. H. Wapstra, and C. Thibault, Nucl. Phys. A **729**, 337 (2003).
[40] S. Goriely [http://www.astro.ulb.ac.be/pmwiki/Brusslib/Hfb17].
[41] S. Raman, C. W. Nestor Jr., and P. Tikkanen, At. Data Nucl. Data Tables **78**, 1 (2001).

[42] A. Bohr and B. R. Mottelson, *Nuclear Structure*, Vol. 2 (Benjamin, New York, Amsterdam, 1974).
[43] D. C. Radford *et al.*, Nucl. Phys. A **752**, 264c (2005).
[44] J. Cederkäll *et al.*, Phys. Rev. Lett. **98**, 172501 (2007).
[45] C. Vaman *et al.*, Phys. Rev. Lett. **99**, 162501 (2007).
[46] A. Ekström *et al.*, Phys. Rev. Lett. **101**, 012502 (2008).
[47] J. E. Wise *et al.*, Phys. Rev. C **45**, 2701 (1992).
[48] J. L. Friar, J. Heisenberg, and J. W. Negele, in *Proceedings of the June Workshop in Intermediate Energy Electromagnetic Interactions*, edited by A. M. Bernstein (Massachusetts Institute of Technology, Cambridge, MA, 1977), p. 325.
[49] I. N. Borzov, E. E. Saperstein, and S. V. Tolokonnikov, Phys. At. Nucl. **71**, 469 (2008).
[50] I. N. Borzov, E. E. Saperstein, S. V. Tolokonnikov, G. Neyens, and N. Severijns, Eur. Phys. J. A **45**, 159 (2010).
[51] M. Honma, T. Otsuka, B. A. Brown, and T. Mizusaki, Phys. Rev. C **69**, 034335 (2004).
[52] P. Vingerhoets *et al.*, Phys. Rev. C **82**, 064311 (2010).
[53] V. G. Soloviev, *Theory of Complex Niclei* (Pergamon, Oxford, 1976).
[54] A. Bohr and B. R. Mottelson, *Nuclear Structure*, Vol. 1 (Benjamin, New York, Amsterdam, 1969).
[55] N. J. Stone, At. Data Nucl. Data Tables **90**, 75 (2005).
[56] S. P. Kamerdzhiev, Sov. J. Nucl. Phys. **9**, 190 (1969).
[57] S. P. Kamerdzhiev, A. V. Avdeenkov, and D. A. Voitenkov, Phys. At. Nucl. **73**, 1478 (2011).